

ND-A149 702

TECHNICAL SUPPORT FOR MICROWAVE EXPERIMENTS ON THE EYE

1/1

LENS(U) SCIENCE APPLICATIONS INC MCLEAN VA

ELECTRO-OPTICS TECHNOLOGY DIV N C WYETH MAR 84

UNCLASSIFIED

DAMD17-80-C-0057

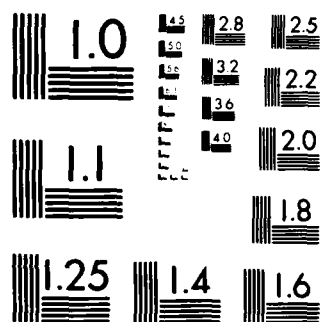
F/G 6/18

NL

END

FORMED

DATE



MICROCOPY RESOLUTION TEST CHART
NATIONAL BUREAU OF STANDARDS-1963-A

AD-A149 702

Technical Support for Microwave Experiments
on the Eye Lens

11

DTIC
ELECTE
JAN 30 1986
S B

DTIC FILE COPY

DISTRIBUTION STATEMENT A
Approved for public release
Distribution Unlimited

Science Applications Incorporated

83 01 02

Technical Support for Microwave Experiments
on the Eye Lens

Final Report

Contract No.: DAMD17-80-C-0057

DTIC
ELECTE
S JAN 30 1985 D
B

SAICTM

Science Applications International Corporation

Post Office Box 1303, 1710 Goodridge Drive, McLean, Virginia 22102, (703) 821-4300

DISTRIBUTION STATEMENT A

Approved for public release
Distribution Unlimited

TECHNICAL SUPPORT FOR MICROWAVE EXPERIMENTS
ON THE EYE LENS

Final Report

N. Convers Wyeth

March 1984

March 1, 1980 to March 1, 1984

Supported by:

U.S. ARMY MEDICAL RESEARCH AND DEVELOPMENT COMMAND
Fort Detrick, Frederick, Maryland 21701
Contract No.: DAMD17-80-C-0057

Science Applications, Inc.
McLean, Virginia 22102

Approved for public release; distribution unlimited.

The findings in this report are not to be construed as an official
Department of the Army position unless so designated by other
authorized documents.

REPORT DOCUMENTATION PAGE		READ INSTRUCTIONS BEFORE COMPLETING FORM
1. REPORT NUMBER	2. GOVT ACCESSION NO. AD A149702	3. RECIPIENT'S CATALOG NUMBER
4. TITLE (and Subtitle) Technical Support for Microwave Experiments on the Eye Lens		5. TYPE OF REPORT & PERIOD COVERED Final Report 3-1-80 to 3-1-84
		6. PERFORMING ORG. REPORT NUMBER
7. AUTHOR(s) N. Convers Wyeth		8. CONTRACT OR GRANT NUMBER(s) DAMD17-80-C-0057
9. PERFORMING ORGANIZATION NAME AND ADDRESS Science Applications, Inc. Electro-Optics Technology Division 1710 Goodridge Drive, McLean, VA 22102		10. PROGRAM ELEMENT, PROJECT, TASK AREA & WORK UNIT NUMBERS 62777A.3E162777A878.BB.014.
11. CONTROLLING OFFICE NAME AND ADDRESS		12. REPORT DATE March 1984
		13. NUMBER OF PAGES 43
14. MONITORING AGENCY NAME & ADDRESS (if different from Controlling Office)		15. SECURITY CLASS. (of this report) Unclassified
		15a. DECLASSIFICATION/DOWNGRADING SCHEDULE
16. DISTRIBUTION STATEMENT (of this Report) Approved for public release; distribution unlimited.		
17. DISTRIBUTION STATEMENT (of the abstract entered in Block 20, if different from Report)		
18. SUPPLEMENTARY NOTES		
19. KEY WORDS (Continue on reverse side if necessary and identify by block number) Laser interferometry; Microwave cataractogenesis; Thermoacoustic waves.		
20. ABSTRACT (Continue on reverse side if necessary and identify by block number) A research program at Walter Reed Army Institute of Research (WRAIR) is concerned with the mechanism by which microwave exposure produces cataracts in the eye lens. Science Applications, Inc. (SAI) has supported WRAIR personnel in system design, equipment assembly, and operation of experiments to measure the physical effects in the eye lens as it is subjected to microwave pulses of varying peak power levels. SAI also developed theoretical models for the thermoacoustic wave phenomena involved and the vibrational motion of the eye lens.		

FOREWARD

Citation of commercial organizations and trade names in this report does not constitute an official Department of the Army endorsement or approval of the products or services of these organizations.



Accession For	
NTIS GRA&I	<input checked="checked" type="checkbox"/>
DTIC TAB	<input type="checkbox"/>
Unannounced	<input type="checkbox"/>
Justification	
By	
Distribution/	
Availability Codes	
Dist	Avail and/or Special
A-1	

SUMMARY

A research program at Walter Reed Army Institute of Research (WRAIR) is concerned with the mechanism by which microwave exposure produces cataracts in the eye lens. Science Applications, Inc. (SAI) has supported WRAIR personnel in system design, equipment assembly, and operation of experiments to measure the physical effects in the eye lens as it is subjected to microwave pulses of varying peak power levels. SAI also developed theoretical models for the thermoacoustic wave phenomena involved and the vibrational motion of the eye lens.

Table of Contents

<u>Section</u>	<u>Page</u>
1 INTRODUCTION AND BACKGROUND	5
1.1 Microwaves and the Eye Lens: the Army Problem	5
1.2 Experiments and Models: the SAI Program	5
2 EXPERIMENTAL MEASUREMENTS	7
2.1 Introduction	7
2.2 Experimental Design Constraints and Choices	7
2.3 System Description	9
2.4 Data Obtained	17
3 THEORETICAL MODELS	22
3.1 Introduction: Goals of the Modeling Effort	22
3.2 Thermoacoustic Waves	22
3.3 Microwave Absorption	23
3.4 Thermoacoustic Wave Equation Solutions	24
3.4.1 One Dimensional Treatment	26
3.4.2 Two Dimensional Treatment	27
3.5 Oscillation of the Eye Lens	34
4 CONCLUSIONS AND RECOMMENDATIONS	36
4.1 Limitations	36
4.2 A Physical Scenario	36
4.3 Recommendations	37
4.4 Postscript	39
REFERENCES	

List of Figures

<u>Figure</u>	<u>Page</u>
2.1 Schematic diagram of the interferometer system	10
2.2 Diagram of the sample chamber design	11
2.3 Schematic diagram of the sample chamber showing laser beam positions for measurements at two different surface points	14
2.4 Interference patterns:	16
(a) adjusted for highest symmetry;	
(b) typical pattern used for motion measurement, with detector size and position shown.	
2.5 CRT output from signal averager: calibrated 2 nm (4 nm peak-to-peak) motion of reference mirror at 1 kHz (no eye lens motion)	18
2.6 CRT output from signal averager: typical eye lens motion signal for a 30 kW, 10 μ sec pulse	20
2.7 Microwave-induced surface displacement data for two points on the same lens	21
3.1 Dynamic pressure vs. time in the saline calculated for a 30 kW, 10 μ sec microwave pulse	32
3.2 Fluid displacement vs. time in the saline calculated for a 30 kW, 10 μ sec microwave pulse	33

1. INTRODUCTION AND BACKGROUND

1.1 Microwaves and the Eye Lens: the Army Problem

Injuries to the eye caused by microwaves have been known for many years (see Reference 1 and citations therein). It has been a generally accepted concept that microwave damage to biological tissues is due almost exclusively to the average temperature elevation which the radiation causes in the tissue. However recent experiments performed at the Walter Reed Army Institute of Research (WRAIR) indicate that additional effects dependent on the modulation of the radiation must also be considered significant in the case of pulsed microwaves such as used in radar.

The WRAIR experiments¹ comprised a parametric study of heat and pulsed microwave energy applied to murine ocular lenses in vitro. The lens showed microscopic physical damage (including cataractogenic changes) after exposure to pulsed microwaves under conditions in which the temperature elevation was essentially negligible. This physical damage, along with an observed dependence on peak pulse power, had led to the hypothesis that the mechanism coupling the microwave radiation to effects in the lens is thermoacoustic transduction.

None of the present safety standards nor any of those under consideration include modulation as a parameter to be considered with respect to potential hazards. Since common land- and ship-based radar systems employ high energy pulses, the possibility that such additional effects may constitute significant safety hazards should be considered. With the use of directive antennas, modern radars can deliver pulse energy densities many times higher than those employed in the WRAIR lens experiments.

1.2 Experiments and Models: the SAI Program

To investigate the hypothesis that thermoacoustic transduction is an important mechanism for eye lens/pulsed microwave interaction,

Science Applications, Inc. (SAI) has collaborated with WRAIR researchers in both experimental measurements and theoretical modeling of the suspected phenomena. The initial lens exposure work at WRAIR involved extracted murine lenses subjected to pulsed microwave radiation while immersed in a small volume of saline solution. Therefore it was desirable to duplicate these conditions while searching for the presence and effects of thermoacoustic transduction. Since initial scoping estimates (later confirmed by detailed calculation) indicated that physical motions of the lens due to thermoacoustic effects would be in the submicron range or smaller, optical interferometry was the measurement system of choice. This was also fully compatible with the requirement of working in a waveguide without altering the microwave mode pattern.

For the experimental measurements, SAI supported WRAIR personnel in the system design, equipment selection and purchase, assembly, and operation of a laser interferometer to detect the movement of the eye lens surface during exposure to pulsed microwaves. This system and its performance is described in Section 2.

SAI has also developed and exercised various theoretical models to describe the absorption of microwaves in the saline volume, the generation and propagation of thermoacoustic waves in the saline, the interaction of these waves with the murine lens, and the subsequent oscillation of the lens in one or more natural modes. This work is summarized in Section 3.

The final section of this report contains an interpretation of the experimental data obtained thus far using the framework of the theoretical modeling work. That is, a physical scenario of the lens/microwave interaction is presented which fits both the experimental findings and the theoretical calculations. This scenario is not uniquely determined, of course, because gaps in both the measurements and the model exist. Therefore Section 4 concludes with an outline of further work needed to substantiate (or disprove) the proposed scenario.

2. EXPERIMENTAL MEASUREMENTS

2.1 Introduction

As described in the previous section, it was desired to examine the physical motion of the surface of murine eye lenses in vitro induced by pulsed microwave radiation. Because motion in the submicron range was expected and because of the necessity to avoid perturbing intracavity microwave fields, optical interferometry was chosen as the measurement technique. The design, operation, and results of the system are described below.

2.2 Experimental Design Constraints and Choices

The rat eye lenses used in the experiment are approximately 3 mm in diameter but contain cell structural dimensions down to sub-micron size (e.g., 15 nm thick membranes). Therefore the system was designed to detect motion down to at least 10 nm using optical interferometry. The choice of the optical system to accomplish this was influenced by a number of experimental constraints.

First, during the microwave pulse exposure and interferometric measurement, the lens had to be immersed in a saline solution to simulate its normal physiological environment. This duplicated conditions used in other lens exposure experiments to which it was desired to relate the results of this work¹, and greatly slowed deterioration of the lens over the period after extraction to the completion of a measurement.

Second, the microwave exposure was to take place within a section of 12.4 x 24.8 cm waveguide (WR-975) fed by a transmitter at one end and having the other end capped with a shorting plate. To make interferometric measurements the eye lens and saline had to be supported within the exposure region without mechanical contact to the waveguide, so that any acoustic noise or equipment movement (e.g., supply cables jerking)

associated with the pulsing of the transmitter would not disturb the position of the lens. Any hole in the side of the waveguide had to be limited to a diameter less than roughly a tenth of the RF wavelength to prevent excessive leakage of microwave power.

The microwave source used was operated at 918 MHz with a pulse width (0.1 μ sec rise time) of 10 μ sec and peak power levels from 10 to 45 kW. Given these excitation parameters and estimates of the mechanical resonance frequencies of the eye lens, it was planned to look for deformation frequencies over a range of 10 Hz to 300 kHz. Since this range includes regions of acoustic and background vibrations in building structures, the interferometer and eye lens had to be isolated mechanically.

A number of optical configurations were considered, each having certain advantages and disadvantages. Deformation of the lens could be detected by measuring how much light from a laser beam it focused through a pinhole at a fixed distance. This would provide a relatively strong (transmission) signal, but interpretation of the data in terms of the magnitude of deformation would not be straightforward. Implementing this scheme with the saline present might also prove difficult. Another arrangement would be to pass a narrow laser beam through the center of the lens (undeviated) and form an interferogram between it and a reference beam. Such a method would have lower sensitivity for the following reason: any change in optical path length through the lens tissue, for example due to foreshortening, would tend to be negated by a simultaneous change in the optical path length through the saline whose index of refraction is quite close to that of the outer layers of the lens.²

Interferometry using light reflected from a small area of the lens surface offers the most direct measurement of surface movement. Unfortunately with the condition of immersion in saline, the reflected signal is quite weak at normal incidence. A glancing angle geometry was considered as a means of increasing the reflected signal strength, but the necessity of additional optics within the waveguide and possibly in the

saline to bring the glancing beam back out from the waveguide and the less straightforward interpretation of the signal were significant disadvantages to this design. The normal reflection mode was chosen as the simplest initial approach, providing the weak signal problems could be overcome. The need to measure the motion at more than one point on the surface was met through use of a small mirror within the chamber (see below).

2.3 System Description

The experimental system was composed of a microwave exposure source, an eye lens sample holder, a basic laser interferometer, and various additional components for adjustment, calibration, and signal detection and processing. Figure 2.1 shows a schematic diagram of the system arrangement.

The microwave source was a transmitter (EPSCO PH-40K) driving a length of WR-975 waveguide. The waveguide was terminated with a shorting plate and included a triple stub tuner between the transmitter and end section. The tuner was adjusted to minimize the (reflected) energy returning from the sample exposure end of the waveguide, thus maximizing the energy deposited in the saline/lens system.

A sample chamber was constructed of plexiglas (microwave transparent) to support the lens and its saline environment in the exposure region of the waveguide. The chamber design is shown in Figure 2.2. The lens was lightly clamped between two 2 mm thick foam rubber pads mounted on opposing plexiglas pedestals. The pedestals and the sides of the chamber were covered with strips of a microwave-transparent acoustical damping material (CP-2, Soundcoat, Inc.) to minimize vibration transmitted to the lens through its mechanical support. The plexiglas panel immediately behind the eye lens was tilted to keep stray reflections out of the return signal path, and black paper (not shown in Figure 2.2) was used to prevent reflection directly from the plexiglas walls. The chamber was designed to be filled with saline to a level sufficient to fully immerse the eye lens; the total volume of saline (50 ml) was large enough to permit coupling over 95% of the microwave energy into the

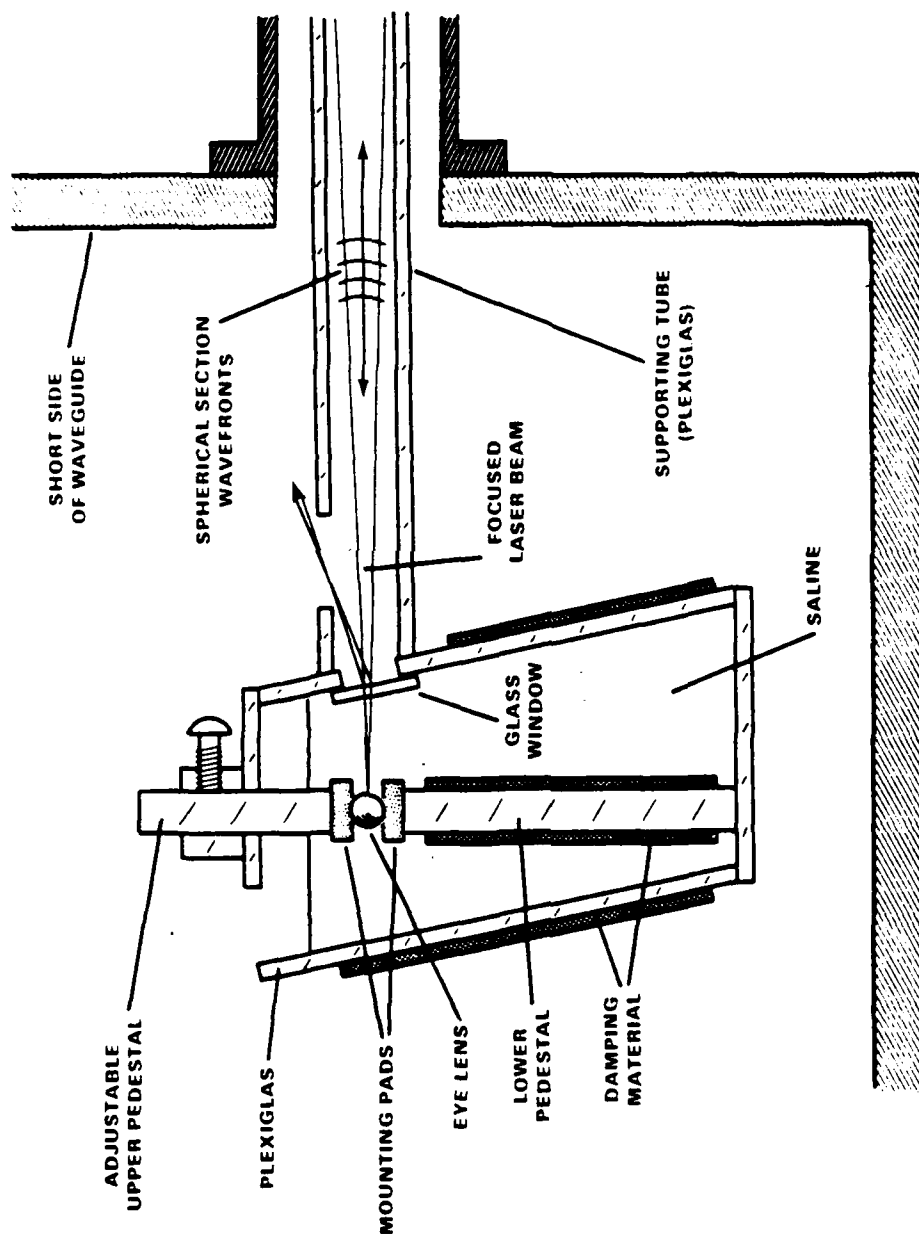


Figure 2.1. Diagram of the Sample Chamber Design.

absorbing media (saline and eye lens). The laser beam entered the chamber through an optically flat ($\lambda/20$) glass window which was also slightly tilted.

The chamber was mounted at the end of a 29 cm long, 1 cm I.D. plexiglas tube whose other end was secured to a vibration-isolation table (NRC RS-46). This plexiglas support tube was oriented to pass without contact through a short section of circular waveguide mounted on a small hole in the short side of the waveguide (see Figure 2.2) thus keeping the chamber and eye lens mechanically isolated from the microwave source (the waveguide and transmitter assembly were not on the vibration-isolation table). The microwave frequency was well below the cutoff of the small circular waveguide thus insuring very low leakage through the hole. The hole was located a distance equal to one fourth the guide wavelength from the shorting end plate to place the sample chamber in the region of maximum electric field strength. The plexiglas tube was also lined with black paper to absorb any stray light and had an opening in the upper side to allow light reflected from the glass window to escape.

The basic laser interferometer components were arranged on the vibration-isolation table as indicated in Figure 2.1. The source was a 15 mW linearly polarized helium-neon laser (Spectra-Physics 124B). Its output beam ($\lambda = 632.8$ nm) was spatially filtered and expanded to roughly one centimeter in diameter. A glass wedge beam splitter with a 50-50 coating was used to split and recombine the object and reference beams. A pellicle-type beam splitter had been tried but contributed excessive signal noise by coupling ambient sound into the light beams. The object beam was focused down the plexiglas tube to the sample chamber by a 350 mm FL lens mounted in a x-y-z adjustable holder on the table. In theory the focusing lens would be adjusted to cause its focal point to coincide with the center of curvature of the area of the eye lens upon which the converging beam is incident. In the approximation that any small area of the eye lens surface is spherical, this alignment would cause the converging wavefronts (seen pictorially in Figure 2.2) to be reflected congruently and would thus return plane waves to interfere with the (plane) reference beam. In actual practice the focusing lens was positioned so that its focal point

was approximately at the physical center of the eye lens and then was adjusted to give the best interference pattern on the observing screen.

With motion measured at only one point on the surface, it is unclear whether the data represents an actual deformation of the lens or simply a change in position of the entire lens. This problem was resolved by using a mirror in the sample chamber to allow the interferometer beam to be reflected from other points on the lens surface as shown in Figure 2.3. A 6.4 mm diameter dielectric layer mirror was mounted using Teflon fixtures for low microwave interaction. An additional piece of black paper was used to intercept the beam transmitted through the lens to prevent bright, extraneous reflections.

The reference beam was manipulated in two ways to enhance the system operation and calibration. As mentioned above the fine adjustment of the object beam on the eye lens was done by visual observation of the interference pattern. Since the visibility of the interference fringes is greatest when the two interfering beams are of equal intensity³, the reference beam had to be attenuated to match the weak reflection from the immersed eye lens during the visual adjustment of the focusing lens. However during a microwave exposure run, the dynamic motion of the eye lens was measured using a small photodiode as described below. This detector was AC-coupled and its signal output increased in proportion to the square root of the reference beam intensity. Thus a technique was needed to vary smoothly the intensity of the reference beam while maintaining the spatial integrity of its wavefronts. This was accomplished by inserting a rotatable half-wave plate (Spectra-Physics 310) and two polarizers (Carl Lambrecht MGTYA20) as shown in Figure 2.1. The reference intensity could be varied from 0% to 100% attenuation by rotating the half-wave plate. The second polarizer was placed in the combined beam leg before the signal detector to filter out any scattered and/or non-polarized light.

The second manipulation of the reference beam involved system calibration. The reference mirror was mounted on a calibrated piezo-

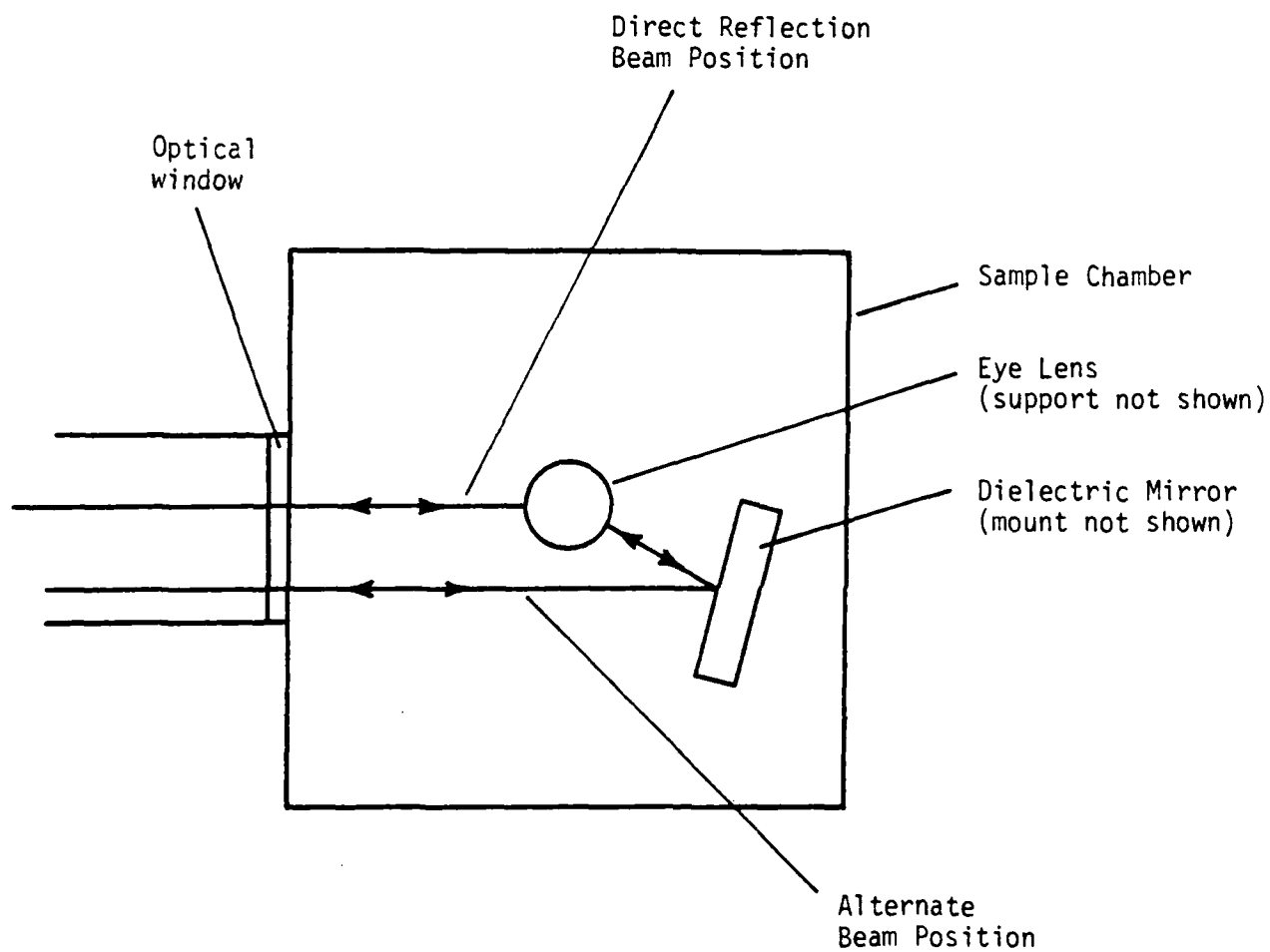


Figure 2.3. Schematic diagram of the sample chamber showing laser beam positions for measurements at two different surface points.

electric translator (Lansing Research, 21.837) which moved the mirror along the reference beam axis in proportion to the voltage applied to it (2.57 nm/volt). With a known amplitude of motion thus imposed on the reference mirror (typically at 1 kHz), it was simple to calibrate the detector output in terms of the displacement it represented for a given fringe pattern. This calibration was then directly applicable to the eye lens signal during a microwave exposure.

The superposition of the reference and object beams on the observing screen produced an interference pattern in a one centimeter diameter circle (the expanded beam size). The width and orientation of the light and dark fringes could be changed by adjusting the angular position of the reference mirror. The full pattern could not be adjusted to all light or all dark, indicating that the converging wave fronts were not exactly aligned with the lens surface. However a highly symmetric pattern of concentric rings with a fairly large central spot was obtainable as shown in Figure 2.4a.

The active area of the photodiode (Motorola MRD510) was a square of dimension 0.5 mm. The best motion signals were obtained when the interference fringes were adjusted as shown in Figure 2.4b, i.e., arcs of small curvature and constant width roughly equal to the detector size.

The light paths of the interferometer were shielded against thermal air currents. However net heating of the saline/lens medium by the microwaves and residual air path effects caused a slow drifting of the interference pattern during an exposure run. When the system was being used to measure motions of less than one fringe width, this drift caused a continuous shift in the intensity variation seen by the detector because the detector aperture was of the order of a fringe width. This was manifest as a varying of the detector AC output down through zero to full inversion (180° phase shift) and back again (a zero level signal would occur when the fringe width and position relative to the detector were such that the part of the fringe intensity distribution moving off the aperture during the vibration cycle was exactly compensated by the part moving onto the

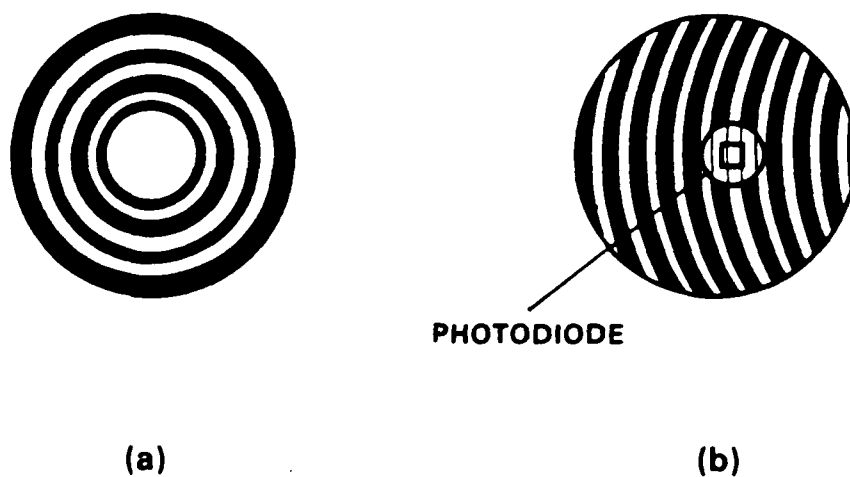


Figure 2.4a & b. Interference Patterns:
(a) adjusted for highest symmetry;
(b) typical pattern used for motion
measurement, with detector size
and position shown.

aperture). By running the piezo-electric reference mirror oscillator during an exposure experiment it was possible to monitor the effects of this unwanted drift and correct for it in the signal processing as described next.

The photodiode output was amplified (Nat. Semi. LF357) to line levels and fed into the various signal processing stages. In a typical run, the microwave transmitter was pulsed at 10 pps and the detector signal stored in a signal averager which was triggered by the transmitter pulse. If the reference mirror oscillation frequency and the transmitter pulse rate were incommensurable, the reference mirror signal was averaged to zero over many pulses along with any other random noise, leaving only those signals correlated with the microwave pulse. However the aforementioned signal inversion drift would tend to cause even these desirable signals to average to zero. Therefore the reference oscillator signal in the fringe motion was observed in real time on an oscilloscope triggered by the piezo-electric translator driver, and the signal averager was activated only when the fringe pattern position was in the proper (chosen) phase. In this way, although the fringe pattern continued to drift during a data run, only signals with a consistent phase were recorded and averaged.

2.4 Data Obtained

The average fringe motion data was stored in digitized form in the signal average and displayed in real time on a CRT screen. For hard copy the stored data was read out to an x-y plotter. Figure 2.5 shows the CRT signal recorded for a calibrated 2 nm motion (at 1 kHz) of the reference mirror and a stationary eye lens (no microwaves). Each point shows the digitized value stored in a channel of the signal averager after averaging 512 signals. The time between channels (sampling interval) is 40 microseconds, and not all channels are shown in these adaptations from the CRT display. The system resolution after signal averaging is clearly excellent at this level.

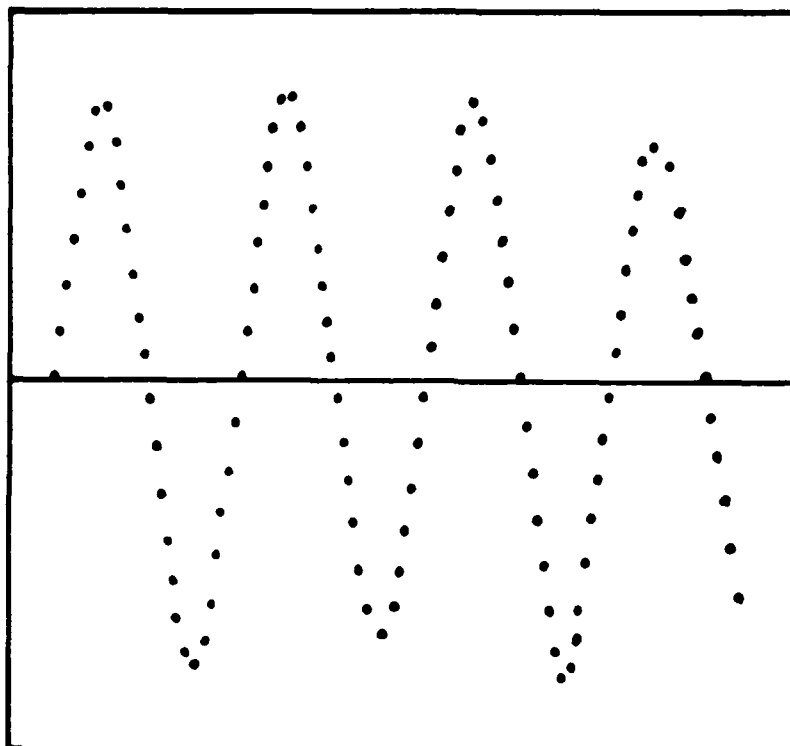


Figure 2.5. CRT output from signal averager: calibrated
2 nm (4nm peak-to-peak) motion of reference mirror at
1 kHz (no eye lens motion).

Figure 2.6 shows a typical averaged signal from an eye lens exposed to a 30 kW microwave pulse. This was obtained with the interferometer beam reflected directly from the lens. The 10 nm scale calibration shown was derived from reference mirror signals similar to Figure 2.5. Significant variations in the magnitude of motion of the surface were seen for different lenses exposed to the same pulse powers. The age of the lenses used and their orientation in the chamber varied also.

The arrangement using a mirror (Figure 2.3) was made operable only at the very end of this contract effort. It proved quite difficult to "find" the surface reflection, i.e., to align the focusing lens-mirror-eye lens system so that an interference pattern was obtained. Data was taken for one lens for both direct and mirror mediated reflections and is shown in Figure 2.7. The lens did have to be reoriented between the runs shown because the zonule ring was obscuring the direct reflection. The magnitude of surface motion seen for both points is small compared with that of Figure 2.6, perhaps because the lens was exposed 24 hours after extraction. However the data does show that the first maxima of both points are in phase, which would not be the case for bulk translation of the lens.

Microwave pulse exposures were also made with the interferometer object beam reflected from the surface of the lower support pedestal and directly from the dielectric mirror. The control data obtained showed negligible motion of the pedestal or the mirror.

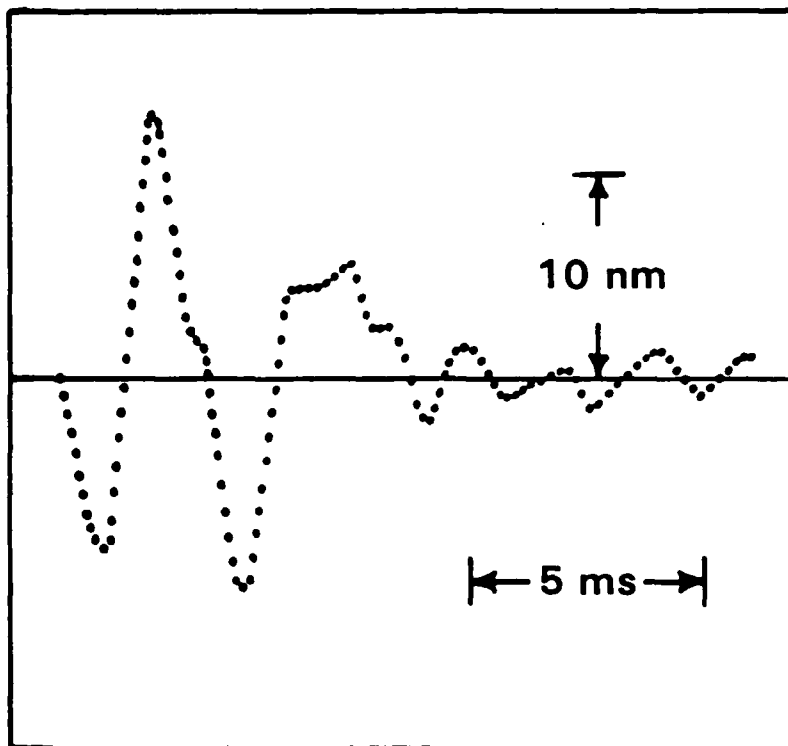


Figure 2.6. CRT output from signal averager:
typical eye lens motion signal for a 30 kW,
10 μ sec pulse.

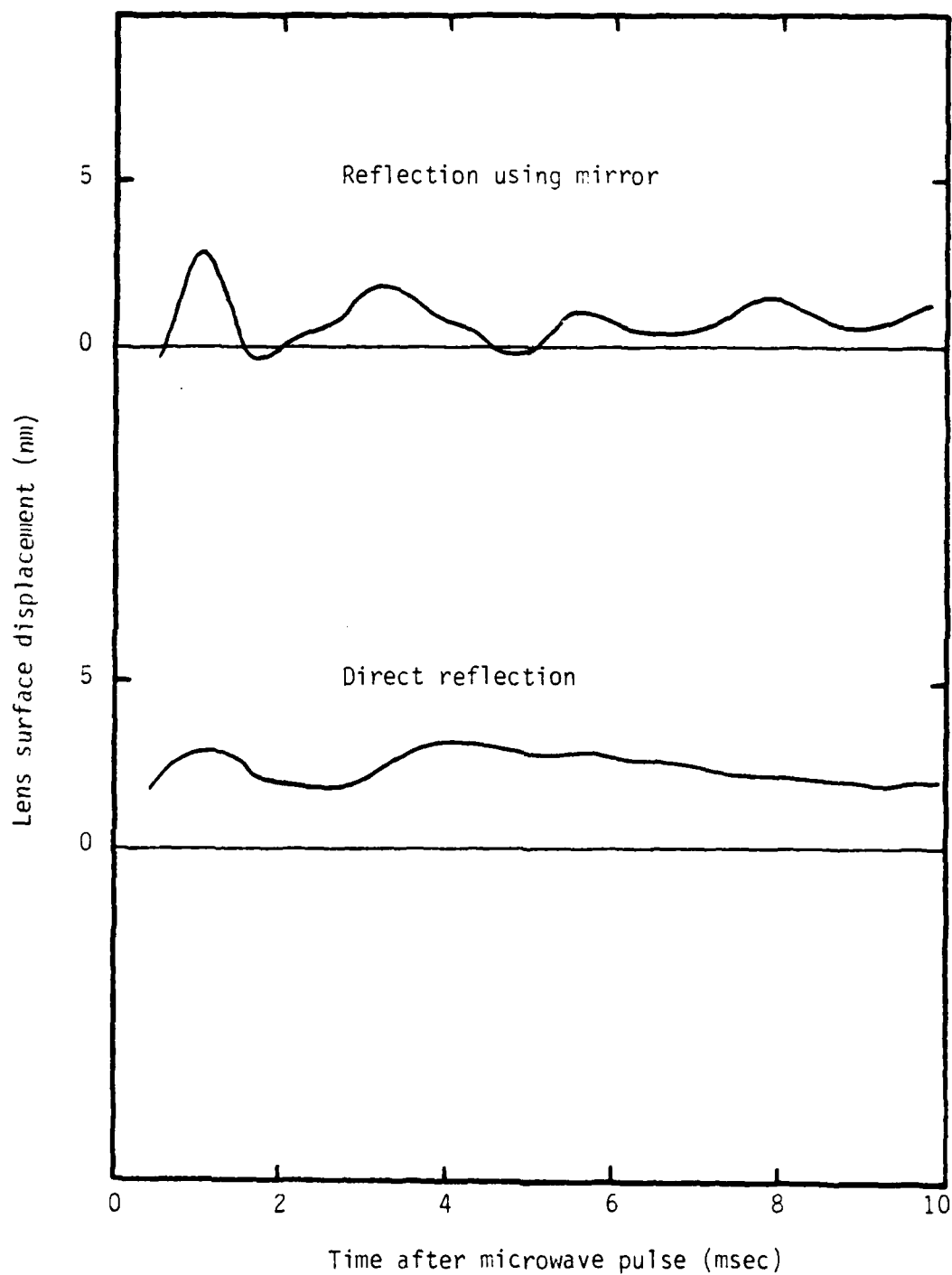


Figure 2.7. Microwave-induced surface displacement data for two points on the same lens.

3. THEORETICAL MODELS

3.1 Introduction: Goals of the Modeling Effort

As the experimental investigation of microwave-induced eye lens motion proceeded, results were obtained which needed to be reconciled with the hypothesis of thermoacoustic transduction as the operant coupling mechanism. In addition more detailed calculations of the magnitude of expected thermoacoustic effects were needed to plan experimental design sensitivities. Another need which arose was the prediction of natural oscillation modes of the eye lens after excitation by a transient force such as a thermoacoustic wave.

3.2 Thermoacoustic Waves

When the equation describing thermal expansion is combined with the relations governing the elastic motion of a medium, the so-called thermo-elastic equations⁴ are obtained. These describe the stress and strain of the medium in time and space as its temperature distribution is changed, including the generation and propagation of thermo-elastic waves. In near isotropic media, such as biological fluids and soft tissues, such thermally produced elastic waves are solely longitudinal⁵ (i.e., irrotational) and at moderate amplitude correspond to ordinary sound waves.

Thermo-elastic waves of significant amplitude are produced when the temperature distribution is changed quickly, and this is usually accomplished experimentally by heating the medium through the absorption of radiation. When the radiation used is visible and near-visible light, the waves (and attendant phenomena) are called optoacoustic or photoacoustic⁶. However the thermo-elastic waves produced by microwave heating of an absorbing medium are usually referred to as thermoacoustic waves.

3.3 Microwave Absorption

To model thermoacoustic effects in the experiments described in Section 2, the first problem which must be treated is the deposition of microwave energy into the saline volume. In a simplified picture the EM radiation fields within the waveguide may be broken down into two plane waves counterpropagating along the axis of the guide. Although a sinusoidal standing wave pattern can be synthesized from these two components, this simplification does not allow for more complicated modal structures such as may result from the presence of the absorbing saline volume. If the x-axis is the axis of propagation with the chamber extending from $x = -\ell$ to $x = +\ell$, the strength of the electric field as a function of position for a wave moving toward negative x is:

$$E_1(x) = E_0 \frac{F(\ell/2)}{1-r^2 F^2(\ell)} \left(F\left(-\frac{x}{2}\right) + r F\left(\frac{x}{2}\right) F(\ell) \right) \quad (3.1)$$

where

$$F(y) \equiv \exp(i2ky - \alpha y)$$

and k is the wave number in the saline, α is the absorption coefficient, r is the reflection coefficient (for e-field, not energy) at the saline surface, and E_0 is the incident field strength. In this treatment the presence of the lens, its supports, and other structures within the saline volume is ignored as a minor perturbation. For the field $E_2(x)$ of the wave propagating toward positive x, the quantity x is replaced by $-x$ in the expression for $E_1(x)$; this neglects the fact that one wave comes directly from the microwave source while the other is a reflection from the shorting end plate and will therefore be downstream from one pass through the chamber. Since the attenuation of the total wave front from one pass is not known, it will be ignored at present. The two field components must be combined to find the energy deposition as a function of position. Although a standing wave is formed by two counterpropagating waves whose phase relationship is constant, the case in which the two waves E_1 and E_2 add

together incoherently (random phase) can also be considered as a means of taking into account the unknown, possibly complex, mode structure in the waveguide cavity. Since the energy absorbed at any point is proportional to the field strength squared, the coherent (fixed phase) case is:

$$I(x) \propto |E_1 + E_2|^2 = E_0^2 D (1 + r e^{\alpha \ell} \cos 2k\ell + r^2 e^{-2\alpha \ell}) (\cosh \alpha x + \cos 2kx) \quad (3.2)$$

and the incoherent case is:

$$I(x) \propto |E_1|^2 + |E_2|^2 = E_0^2 D \left[(1 + r^2 e^{-\alpha \ell}) \cosh \alpha x + (4r e^{-\alpha \ell} \cos 2k\ell) \cos 2kx \right] \quad (3.3)$$

where

$$D = 2e^{-\alpha \ell} / (1 - 2r^2 e^{-2\alpha \ell} \cos 4k\ell + r^4 e^{-4\alpha \ell})$$

Thus the heat production rate as a function of position is

$$R(x) = \alpha I(x) = \alpha I_0 \left[A \cosh \alpha x + B \cos 2kx \right] \quad (3.4)$$

where I_0 is the incident microwave power, and A and B are coefficients containing the α , ℓ , k , and r dependence shown in the previous equations (note that for the coherent case, $A = B$).

3.4 Thermoacoustic Wave Equation Solutions

With the heat production rate as a function of position now specified, the temperature, T , as a function of time and position can be found using the heat conduction equation:

$$\rho C_p \frac{\partial T}{\partial t} - \chi \nabla^2 T = \alpha I(x, t) \quad (3.5)$$

where ρ is the saline density, C_p is the specific heat, and λ is the thermal conductivity. For transient thermoacoustic phenomena occurring in milliseconds, the effects of heat diffusion can be ignored (adiabatic limit) for saline, leaving the temperature solution as:

$$T(x,t) = (\alpha t / \rho C_p) I(x) \quad (3.6)$$

When the microwave pulse (which began at $t = 0$) is completed at $t = \tau$, the temperature can be written as

$$T(x) = (\alpha \tau / \rho C_p) I(x) \quad (3.7)$$

until heat diffusion becomes noticeable.

For thermoacoustic wave generation and propagation in a liquid medium (shear modulus vanishing), the governing equation is:⁷

$$\nabla^2 \vec{u} - \frac{1}{c^2} \frac{\partial^2 \vec{u}}{\partial t^2} = \epsilon \vec{\nabla} T \quad (3.8)$$

where \vec{u} is the displacement, c is the speed of sound (equal to $\sqrt{B/\rho}$ where B is the modulus of elasticity), and ϵ is the coefficient of thermal expansion. Since \vec{u} is irrotational for longitudinal sound waves such as are produced by temperature variations, scalar potentials may be used such as ψ and ϕ , with $\vec{u} = \vec{\nabla} \psi$ and $\frac{\partial \vec{u}}{\partial t} = \vec{\nabla} \phi$ with $\phi = \frac{\partial \psi}{\partial t}$. The potential ϕ is convenient for liquids because the acoustic pressure p is given by:

$$p = -\rho \frac{\partial \phi}{\partial t} \quad (3.9)$$

Therefore the present problem of microwave-generated thermoacoustic waves in the saline-filled sample chamber was modeled by solving the equation

$$\nabla^2 \phi - \frac{1}{c^2} \frac{\partial^2 \phi}{\partial t^2} = \epsilon \frac{\partial T}{\partial t} \quad (3.10)$$

with appropriate initial and boundary conditions.

The theoretical work in this area was reviewed,⁵⁻¹⁰ and various derived expressions were used for order of magnitude effects prediction. However the case of a confined fluid volume with moderate radiation absorption constants was not treated. Since the finite wall separation was certain to introduce important differences from the standard semi-infinite medium case, an effort was made to model the thermoacoustic waves in the specific case of the sample chamber saline volume.

3.4.1 One Dimensional Treatment

The temperature distribution, as explained above, was assumed to vary only along the waveguide axis (x-axis) in the adiabatic limit. Since acoustic waves in a duct of transverse dimensions much smaller than their wavelength may be approximated by plane waves,¹¹ it was decided initially to model the thermoacoustic waves in the sample chamber in one dimension, i.e., as plane waves propagating parallel to the waveguide axis. The equation for c was solved analytically and evaluated using typical experimental parameter values. The results showed induced pressure waves of moderate magnitude but fluid displacements of less than 5 picometers. These results were felt to be an artifact resulting from confining the fluid to expansion in only one dimension between two fixed end walls. An attempt was made to remedy this deficiency by introducing the effects of the free upper surface through an open channel distensibility term¹² added to the saline compressibility. However this type of approximation was not appropriate to the fast time scales of the pulsed microwave heating case. Furthermore, for the case of a one dimensional medium with fixed end walls as the boundary conditions, it can be shown that any thermo-elastic wave generation is dependent on a spatial gradient of heat production and that no waves are produced by uniform heating of the medium.

For 918 MHz and saline, α^{-1} is approximately 5 cm so that there is some variation across a 2 cm wide chamber due to absorption alone. The wavelength is about 5 cm in the saline so the variation due to standing wave effects is comparable. However it is important to realize

that if the one dimensional model were used in the case of negligible spatial variation of heat production, it would predict no thermoacoustic effect when in fact the free (upper) surface of the saline volume allows wave generation even for uniform heating.

3.4.2 Two Dimensional Treatment

In view of the aforementioned shortcomings of the one dimensional model, it was decided to solve the thermoacoustic wave equation in a two dimensional treatment of the saline chamber volume. The horizontal axis perpendicular to the waveguide axis was the direction along which negligible variation in all quantities was assumed. The fluid was assumed to be confined between fixed walls along the waveguide axis and to be bounded by a fixed bottom wall and a free upper surface along the vertical axis.

The initial conditions for solving Equation 3.10 were that c and its time derivatives and T (the excess temperature above initial, uniform temperature T_0) were zero. The boundary conditions were set for a volume with rigid walls at $x = \pm x$ and $y = 0$ and a free surface at $y = h$. Since $v_x = \partial\phi/\partial x$ and $v_y = \partial\phi/\partial y$, this gives

$$\left. \frac{\partial\phi}{\partial x} \right|_{x = \pm x} = 0 \quad (3.11)$$

$$\left. \frac{\partial\phi}{\partial y} \right|_{y = 0} = 0 \quad (3.12)$$

for the rigid wall boundary conditions. For the free surface at $y = h$, it may be shown that:¹³

$$\left. \frac{\partial^2 \phi}{\partial t^2} \right|_{y=h} = -g \left. \frac{\partial \phi}{\partial y} \right|_{y=h} \quad (3.13)$$

for a fluid in a gravitational field with acceleration g . Using Eqns. 3.4, 3.6, and 3.7, the right-hand side of Eqn. 3.10 becomes

$$\frac{\partial T}{\partial t} = \begin{cases} \sum_{i=1,2} F_i \cos b_i x & 0 < t < \tau \\ 0 & t > \tau \end{cases}$$

with $F_1 = (\beta \alpha / \rho C_p) I_0 A$

$$b_1 = i\alpha$$

$$F_2 = (\beta \alpha / \rho C_p) I_0 B$$

$$b_2 = 2k$$

A Laplace transform is used to transform $\phi(x,y,t)$ to $\bar{\phi}(x,y,s)$ and Eqn. 3.10 becomes:

$$c^2 \nabla^2 \bar{\phi} - s^2 \bar{\phi} = (1 - e^{-s\tau}) \frac{c^2}{s} \sum_i F_i \cos b_i x \quad (3.14)$$

The rigid wall conditions (Eqns. 3.11 and 3.12) become simply:

$$\left. \frac{\partial \bar{\phi}}{\partial x} \right|_{x=\pm l} = 0 \quad (3.15)$$

$$\left. \frac{\partial \bar{\phi}}{\partial y} \right|_{y=0} = 0 \quad (3.16)$$

At $y = h$, Eqn. 3.13 becomes:

$$s^2 \tau(y=h) = -g \frac{\partial \tau}{\partial y} \Big|_{y=h} \quad (3.17)$$

However, under the condition $gh \ll c^2$, which is easily satisfied for a chamber height $h = 5$ cm and longitudinal sound velocity in water of 1.5×10^5 cm/sec, Eqn. 3.17 becomes equivalent to:

$$\tau(y=h) = 0 \quad (3.18)$$

The solution for τ was found as:

$$\begin{aligned} \tau(x,y,s) = & -c^2(1-e^{-s\tau}) \sum_i F_i \left[\frac{\cos b_i x}{s^2(s^2 + b_i^2 c^2)} + \frac{b_i c \sin b_i \ell \cosh sx/c}{s^2(s^2 + b_i^2 c^2) \sinh s\ell/c} \right. \\ & - \frac{\sin b_i \ell}{b_i \ell} \frac{\cosh sy/c}{s^3 \cosh sh/c} - \left(\frac{c}{\ell}\right)^2 2b_i \ell \sum_{n=1}^{\infty} \left\{ (-1)^n \frac{\cosh \left[(s^2 + (\frac{n\pi c}{\ell})^2)^{1/2} \frac{y}{c} \right]}{\cosh \left[(s^2 + (\frac{n\pi c}{\ell})^2)^{1/2} \frac{h}{c} \right]} \right. \\ & \left. \left. \times \frac{\cos(n\pi x/\ell)}{s(s^2 + (\frac{n\pi c}{\ell})^2) (b_i^2 c^2 - (\frac{n\pi c}{\ell})^2)} \right\} \right] \quad (3.19) \end{aligned}$$

After performing the inverse Laplace transform, the solution for the velocity potential $\phi(x,y,t)$ was found. The multiplying term $(1-e^{-s\tau})$ in $\tau(x,y,s)$ in Eqn. 3.19 allows the solution for ϕ to be written as:

$$\phi(x,y,t) = \phi'(x,y,t) - U(t-\tau) \phi'(x,y,t-\tau) \quad (3.20)$$

where

$$U(t-\tau) = \begin{cases} 0 & \text{for } t < \tau \\ 1 & \text{for } t > \tau \end{cases}$$

i.e., U is the unit step function. The originating function ϕ' is given by:

$$\begin{aligned} \phi'(x,y,t) = & -c^2 \sum_{i=1,2} F_i \left\{ \frac{\sin b_i \xi}{b_i \xi} \left[\frac{h^2 - y^2}{2c^2} + \frac{8h^2}{c^2} (F(y_+/2h) + F(y_-/2h)) \right] \right. \\ & + 2b_i \xi \sin b_i \xi \left(\frac{c}{\xi} \right)^2 \sum_{n=1}^{\infty} (-1)^n \frac{\cos(n\pi x/\xi)}{(b_i c)^2 - (n\pi c/\xi)^2} \left[\frac{1 - \frac{\cosh(n-y/\xi)}{\cosh(n-h/\xi)}}{(n\pi c/\xi)^2} + \right. \\ & \left. \left. \frac{4}{\pi} \sum_{p=1}^{\infty} (-1)^p \frac{\cos Lt \cos((2p-1)\pi y/2h)}{(2p-1)L^2} \right] \right\} \end{aligned} \quad (3.20)$$

where

$$(F(y_+/2h) + F(y_-/2h)) \equiv \frac{2}{\pi^3} \sum_{n=1}^{\infty} \frac{(-1)^n}{(2n-1)^3} \cos((2n-1)\pi y/2h) \cos((2n-1)\pi ct/2h)$$

and

$$L^2 \equiv (c\pi/\xi)^2 (n^2 + (\xi/2h)^2 (2p-1)^2)$$

Applying Eqn. 3.9 to Eqn. 3.20 and using the fact that $\phi' = 0$ for $t = 0$ gives the following expression for the dynamic pressure:

$$p(x,y,t) = p'(x,y,t) - U(t-\tau)p'(x,y,t-\tau) \quad (3.21)$$

where

$$\begin{aligned} p'(x,y,t) = & \rho c^2 \sum_i F_i \left\{ \frac{\sin b_i \xi}{b_i \xi} \frac{4h}{c} \left[F'(y_+/2h) - F'(y_-/2h) \right] \right. \\ & - 2b_i \xi \sin b_i \xi \left(\frac{c}{\xi} \right)^2 \sum_{n=1}^{\infty} (-1)^n \frac{\cos(n\pi x/\xi)}{(b_i c)^2 - (n\pi c/\xi)^2} \frac{4}{\pi} \sum_{p=1}^{\infty} (-1)^p \frac{\sin Lt \cos((2p-1)\pi y/2h)}{(2p-1)L} \left. \right\} \end{aligned}$$

and

$$F'(y_+/2h) - F'(y_-/2h) \equiv - \frac{c}{h\pi^2} \sum_{n=1}^{\infty} \frac{(-1)^n}{(2n-1)^2} \cos((2n-1)\pi y/2h) \sin((2n-1)\pi ct/2h)$$

From the original definition of \vec{c} , the expression for displacement is seen to be given by:

$$\vec{u} = \int_0^t dt \vec{v}_c \quad (3.22)$$

For example the displacement in the x-direction is given by:

$$u_x(x,y,t) = u'_x(x,y,t) - U(t-\tau)u'_x(x,y,t-\tau) \quad (3.23)$$

where

$$u'_x = c^2 \sum_i F_i \frac{2b_{i,x} \sin b_{i,x}}{(b_{i,c})^2 - (n\pi c/L)^2} \sum_{n=1}^{\infty} (-1)^n \frac{n \sin(n\pi x/L)}{(b_{i,c})^2 - (n\pi c/L)^2} \\ \times \left[\frac{t(1 - \frac{\cosh(n\pi y/L)}{\cosh(n\pi h/L)})}{(n\pi c/L)^2} + \frac{4}{\pi} \sum_{p=1}^{\infty} (-1)^p \frac{\sin Lt \cos((2p-1)\pi y/2h)}{(2p-1)L^3} \right]$$

Examination shows that the sums in the expressions for pressure and displacement converge fairly rapidly. Eqns. 3.21 and 3.23 were evaluated over a sequence of times for a set of representative parameter values using a computer to perform the summations to reasonable accuracy. Typical results are shown in Figures 3.1 and 3.2.

The calculations shown in Figures 3.1 and 3.2 were made assuming a 30 kW, 10 μ sec microwave pulse of wavelength 5 cm (in saline) absorbed by a $2 \times 2 \times 5$ cm³ chamber with an absorption coefficient of 0.2 cm⁻¹ and a reflection coefficient (electric field) at the walls of 0.64.

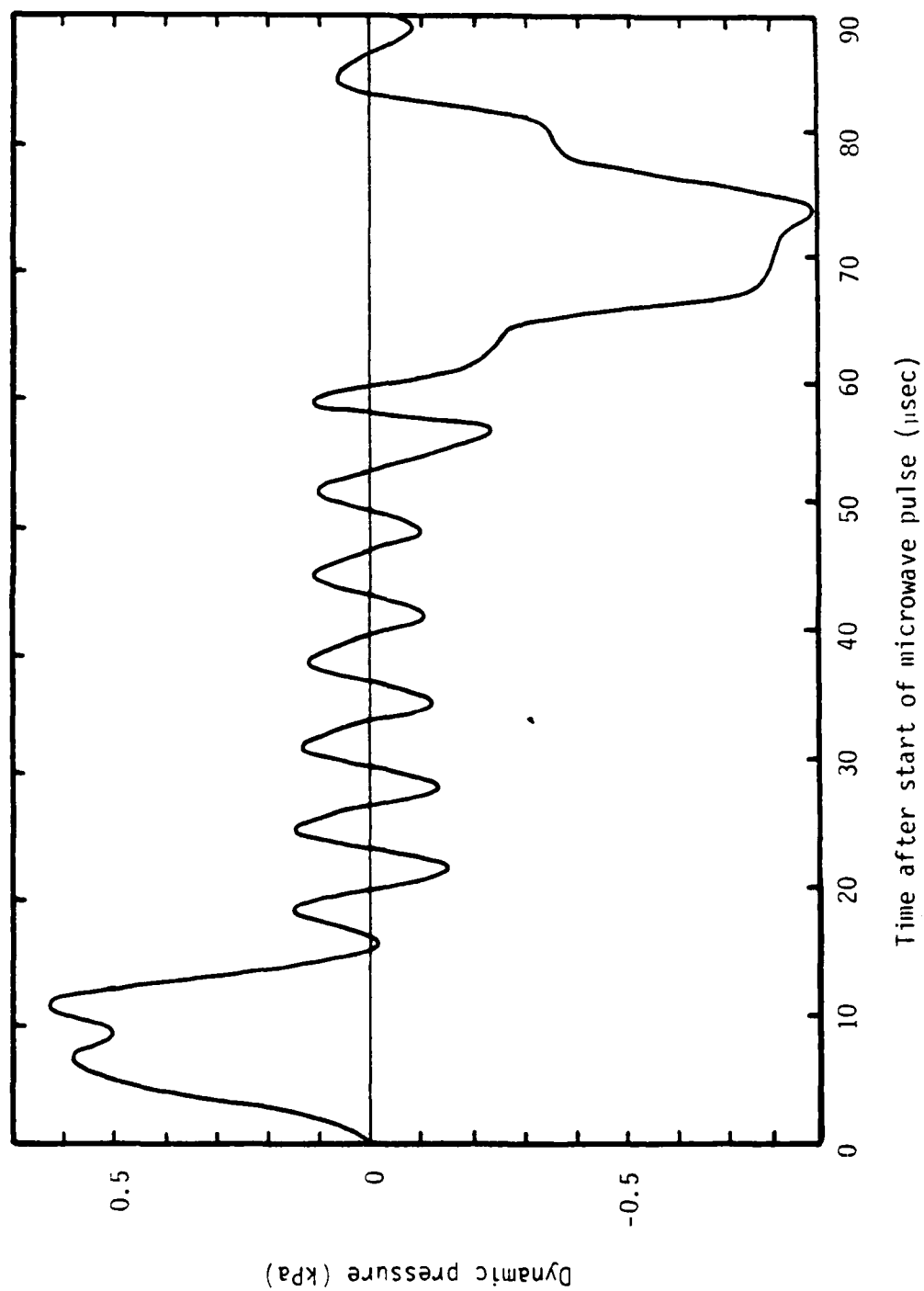


Figure 3.1. Dynamic pressure vs. time in the saline calculated for a 30 kW, 10 μsec microwave pulse.

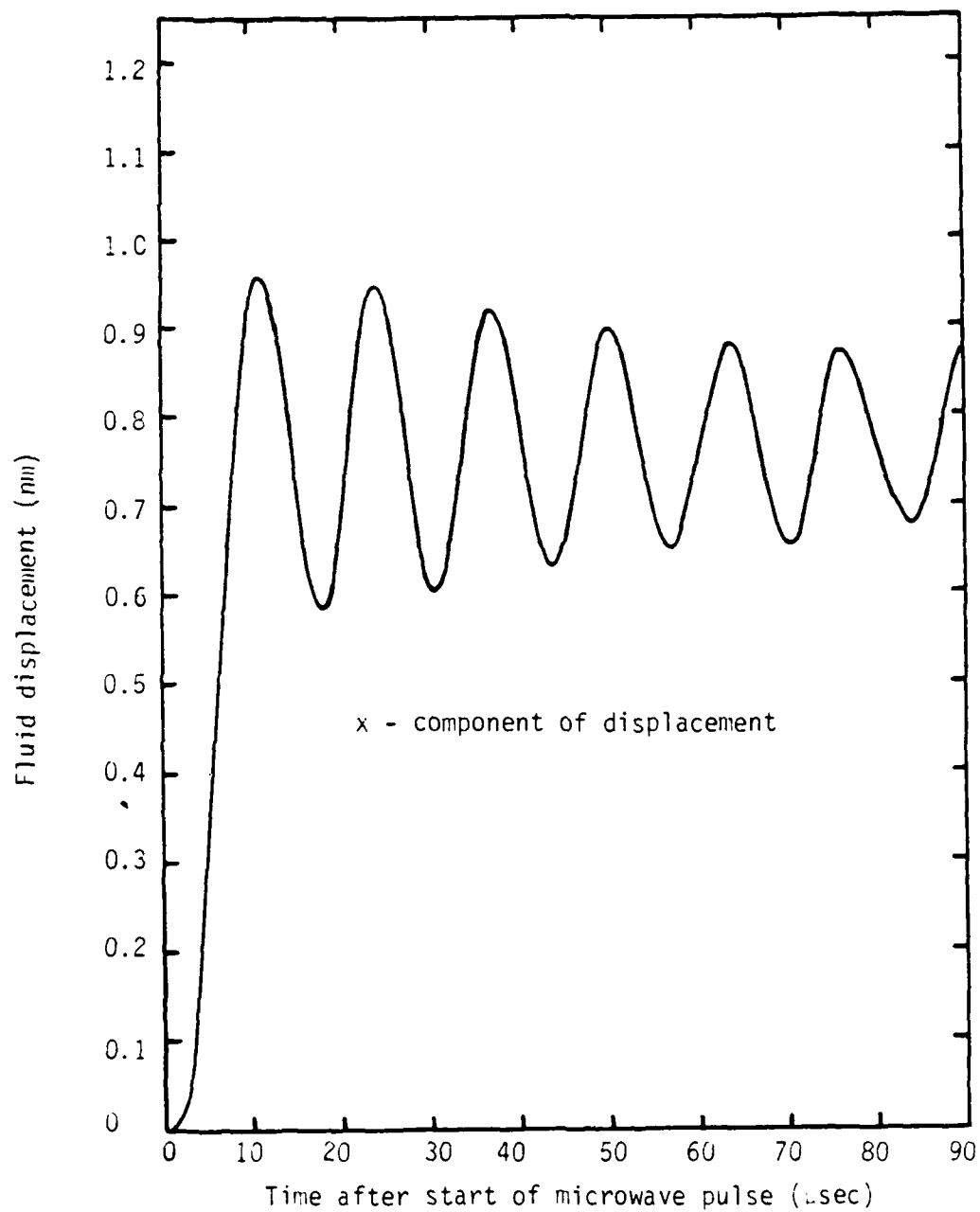


Figure 3.2. Fluid displacement vs. time in the saline calculated for a 30 kW, 10 μ sec microwave pulse.

The sound speed was taken as 1.5×10^5 cm/sec, and the pressure and fluid displacement are calculated for a position 4 cm from the bottom (1 cm below the surface) and displaced 0.5 cm in the x-direction from the center vertical axis of the chamber. Both figures represent calculations made using the incoherent electric field distribution (Eqn. 3.3). In fact in the several computer runs made, no qualitative difference between the incoherent and coherent cases was seen as reflected in the pressure and displacement results; the quantitative differences were less than a factor of two. The pressure curve in Figure 3.1 can be explained qualitatively as follows. An initial increase in pressure is seen which is a combination of a wave originating from the nearest end wall and dependent on the spatial variation of the temperature distribution (x-direction) and a larger pressure wave caused by the free surface one centimeter (6.7 μ sec) away (y-direction). The other end wall wave arrives at the end of the initial overall pulse ($\sim 13 \mu$ sec), and subsequently alternate waves from the two end walls bounce back and forth creating a standing wave of period $\sim 6.7 \mu$ sec. After another 50-60 μ sec the large pulse returns with inverted phase after reflection from the fixed bottom. With no dissipative terms included in the model, this behavior would continue with the appropriate periodicity. The x-component of displacement shown in Figure 3.2 is proportional to the pressure gradient in the x-direction and as such does not show directly the effects of the pressure waves traveling in the y-direction. The period is twice that of the standing pressure waves in the x-direction.

The dissipation or damping of these thermoacoustically generated waves has not yet been quantitatively addressed. Energy will be lost through a combination of viscous damping (heat generation) in the fluid, radiation through the free surface coupling to the air above, and some flexing of the assumed rigid chamber walls.

3.5 Oscillation of the Eye Lens

With the above results of calculation of the pressure waves in the sample chamber, it became necessary to consider the effects on the eye lens. Specifically the question arose: why are the lens surface motions

observed at a much lower frequency than the calculated pressure/displacement waves (500 Hz vs. 100 kHz)? The displacements observed were somewhat larger than calculated but not to the extent of the frequency discrepancy.

As a first approximation toward calculating its vibration characteristics, the eye lens may be treated as a homogeneous elastic sphere. The oscillatory modes of such a body have been calculated in detail.¹⁴ In the original proposal for this program of investigation, the frequency of the lowest order, purely compressional mode was estimated to be on the order of hundreds of kilohertz for a sphere the size of the murine lens with the compressibility of typical biological tissue (close to that of water). However, other modes of lower specific energy exist which involve elastic deformation without compression.¹⁴ The lowest order frequencies of these modes are in the hundreds of hertz range for the homogeneous eye lens model. These modes also have the property that they can be excited in a sphere by an incident plane wave in the surrounding medium.¹⁵ It would be inappropriate to present these solutions in detail here because their application to the thermoacoustic wave/eye lens problem has not yet been worked out. A hypothetical scenario based on the ideas covered here will be presented in Section 4.

It should also be noted that the oscillatory modes of a spherical droplet whose motion is governed by surface tension have also been worked out.¹⁶ If it were to be found that the deformation of the lens body were mainly governed by the elastic properties of the lens capsule, these solutions would be used to predict the natural oscillation frequencies. The frequency of the lowest order mode is given by:¹⁶

$$f = \sqrt{\frac{2\alpha}{\pi \rho R^3}} \quad (3.24)$$

where α is the surface tension, ρ is the density, and R is the radius. From observation during handling, it appears that the lens capsule has a restoring force or "surface tension" of the order of magnitude of a drop of water. If the value of α for water is used, the above equation predicts a lowest frequency for a sphere like the lens of a few hundred hertz.

4. CONCLUSIONS AND RECOMMENDATIONS

4.1 Limitations

In the following parts of this concluding section, a hypothetical scenario will be presented to explain the experimental data in terms of the theoretical modeling results. However, it is clear from the descriptions of Section 2 above that substantially more measurements must be taken to define with any certainty the overall motion of the eye lens surface after microwave pulse exposure. Data on motion during the first 500 microseconds is also lacking due to equipment limitations. In addition, several key parts of the modeling effort such as the coupling of the plane thermoacoustic (compressional) waves to the low frequency (non-compressional) vibration modes of the eye lens sphere have yet to be worked out in detail. Finally many of the assumptions used in the modeling effort need to be checked by experimental measurement (e.g., determine the actual coefficient of restitution of a murine lens); these needs will be listed in the recommendations given below.

With an awareness of these clear limitations of both the present experimental data and the theoretical modeling effort, the following scenario is described. It is certainly not the only possible explanation of the unrestrictive data points, but seems to be a probable one in the context of the theoretical results.

4.2 A Physical Scenario

As the microwave pulse arrives at the shorted end of the waveguide containing the saline-filled sample chamber, a mode structure with strong coupling into the absorbing fluid (reflected power down by 10-12 dB) is established in a time of order of the wave period (~ 1 nsec). The microwave energy is deposited in the absorbing media (saline and lens) as two counter-propagating waves along the waveguide (x-direction) axis.

Through the well-known thermoacoustic effect, this heating by the microwaves produces plane acoustic waves propagating through the saline. These include both waves traveling along the x-axis, caused by the spatial variation in thermal expansion against rigid walls, and waves traveling in the vertical (y-axis) direction, caused by thermal expansion with a free surface. For purposes of the initial generation and propagation of these waves, the eye lens is indistinguishable from the saline fluid with similar absorptive and compressional properties.

However the eye lens tissue also has a finite elastic shear modulus, a quantity which is essentially zero for the saline. While the high frequency acoustic waves are quickly damped in the lens, the continuing impact of the wall-reflected acoustic waves in the saline excites fundamental, low frequency spheroidal oscillations of the lens body in which the energy is stored as equivoluminal elastic distortion rather than compressional changes. There may also be a coupling, subject to symmetry constraints, of the initial compression waves in the lens directly to the equivoluminal modes. Although the fast thermoacoustic waves in the chamber decay away fairly quickly, the eye lens continues with an observable low frequency oscillation for several milliseconds. These oscillation modes have an axial symmetry consistent with plane wave excitation and with support of the sphere at one or two diametrically opposed points.

Since these low frequency, equivoluminal oscillations could be expected to occur during the normal mechanical shocks of the organism's life, the cataractogenic damage observed in the microscopic studies is most likely caused by the initial compressional acoustic waves as they pass through the lens.

4.3 Recommendations

By using the above scenario as a working hypothesis, a number of recommendations can be made for both experimental and theoretical work to confirm, modify, or deny its various tenets. Experimentally, a number of

questions could be answered if the putative thermoacoustic waves in the chamber were directly detected. Their frequency, amplitude, and decay rate are all desired quantities. It is also very desirable to obtain data on the elastic constants of the murine lens either by experimental measurement or literature search. Lastly, as a continuation of the present experiments, more data on the eye lens surface motion at different points should be taken to define the oscillation mode, and the first 500 microseconds after the start of the microwave pulse should be examined to see if the initial thermoacoustic impulses can be detected. Also of interest would be an experiment designed to enhance the excitation of the low frequency lens mode by operating the transmitter in a burst mode in which the microwave pulses arrive in a short train whose pulse separation time matches the mode period.

In the area of theoretical calculations and modeling, an estimate of the acoustic wave decay rate due to dissipative processes is needed for the conditions involved. Also the two proposed mechanisms for excitation of the low frequency lens modes - coupling from a lens compressional mode and coupling from an external acoustic wave - must be modeled with some detail to get estimates on the amplitudes expected and the transition times involved.

Ultimately, of course, the question of the lens' nonhomogeneous structure¹⁷ must be addressed. This aspect of the problem is fundamental to understanding how the acoustic waves cause damage to the lens structures. Experiments in which lenses (in vitro or in vivo) were subjected to acoustic waves generated by means other than microwaves but matching the thermoacoustic frequencies and amplitudes might be contemplated as a means of confirming the nature of the damage mechanism.

4.4 Postscript

All of the work described in this report, both experimental and theoretical, has centered on the exposure in vitro of murine eye lenses to pulsed microwaves. Specifically, the extracted lenses were exposed while immersed in a small volume of saline solution. This arrangement was used to closely duplicate the original work which found precataractous damage due to pulsed microwaves.¹

Ultimately, however, these results must be related to the Army problem as described in Section 1 and therefore to eye lens exposure in vivo. In the human eye, the lens is virtually surrounded by fluids: the anterior surface by the aqueous humor and the posterior surface by the vitreous humor. Thus under pulsed microwave exposure the lens could be subject to extrinsic thermoacoustic waves generated in the humors. However, as the dimensions are smaller, the generation of thermoacoustic waves due to spatial variation in heat deposition becomes less effective. Nevertheless the other mechanism seen in the saline volume case, namely generation of waves from the free surface, will be operable in the situation in vivo also. A totally "free" (pressure equal zero) surface is not required; only one which can move or flex in response to an increase in pressure. The schlera, which maintains its shape mostly by the internal pressure of the eye fluids,¹⁸ fits this description.

So does the capsule of the lens itself, which leads naturally to the question of intrinsic thermoacoustic waves generated within the lens itself. This issue was not addressed in the physical scenario presented above in which no distinction was made between the surrounding saline and the lens during the wave generation process. Since the lens capsule does in fact constitute a flexible yet resilient boundary, it is clear that intrinsic thermoacoustic effects are possible. Their presence and magnitude could be estimated if the mechanical properties of the lens and its capsule were known and perhaps detected by surface motion measurements on a naked lens during microwave pulse exposure.

REFERENCES

1. P.J. Stewart-Dehaan, M.O. Creighton, L.E. Larsen, J.H. Jacobi, W.M. Ross, M. Sanwal, T.C. Guo, W.W. Guo, and J.R. Trevithick, Exp. Eye Res. 36, 75 (1983).
2. M.C.W. Campbell and A. Hughes, Vision Research 21, 1129 (1981).
3. M. Born and E. Wolf, Principles of Optics (MacMillan Company, New York, 1964) Chapter VII.
4. A.E.H. Love, A Treatise on the Mathematical Theory of Elasticity (Dover, New York, 1944) p. 108.
5. P. Chadwick and I.N. Sneddon, J. of Mech. and Phys. of Solids 6, 223 (1958).
6. C.K.N. Patel and A.C. Tam, Rev. of Mod. Phys. 53, 517 (1981).
7. G. Liu, Applied Optics 21, 955 (1982).
8. J.C. Lin, Microwave Auditory Effects and Applications, (Charles C. Thomas, Springfield, Illinois, 1977) pp. 99-134.
9. L.S. Gournay, J. Acoustical Soc. of Amer. 40, 1322 (1966).
10. R.M. White, J. Appl. Phys. 34, 3559 (1963).
11. L.E. Kinsler, et al., Fundamentals of Acoustics (J. Wiley & Sons, New York, 1982) pp. 216-222.
12. J. Lighthill, Waves in Fluids (Cambridge University Press, New York, 1979) pp. 89-96.
13. Ibid, pp. 207-208.
14. A.C. Eringen and E.S. Suhubi, Elastodynamics (Academic Press, New York, 1974) Volume II, pp. 804-862.
15. Ibid, pp. 911-919.
16. L.D. Landau and E.M. Lifshitz, Fluid Mechanics (Addison-Wesley, Reading, Massachusetts, 1959) pp. 238-240.
17. H. Bloemendal (editor), Molecular and Cellular Biology of the Eye Lens (J. Wiley & Sons, New York, 1981).
18. D. Sliney and M. Wolbarsht, Safety with Lasers and Other Optical Sources (Plenum Press, New York, 1980) pp. 65-76.

Bibliography of Publications supported by the Contract:

- (1) "Laser interferometer for measuring microwave-induced motion in eye lenses in vitro" by P.V.K. Brown and N.C. Wyeth, Review of Scientific Instruments, 54, 85 (1983).

List of Personnel who received contract support:

N. Convers Wyeth
J. Knotts
W. Koechner

DISTRIBUTION LIST

12 copies	Director Walter Reed Army Institute of Research Walter Reed Army Medical Center ATTN: SGRD-UWZ-C Washington, DC 20307-5100
4 copies	Commander US Army Medical Research and Development Command ATTN: SGRD-RMS Fort Detrick, Frederick, Maryland 21701-5012
12 copies	Defense Technical Information Center (DTIC) ATTN: DTIC-DDAC Cameron Station Alexandria, VA 22304-6145
1 copy	Dean School of Medicine Uniformed Services University of the Health Sciences 4301 Jones Bridge Road Bethesda, MD 20814-4799
1 copy	Commandant Academy of Health Sciences, US Army ATTN: AHS-CDM Fort Sam Houston, TX 78234-6100

END

FILMED

2-85

DTIC